Inhibition of Lymphangiogenesis and Angiogenesis in Breast Tumor Xenografts and Lymph Nodes by a Peptide Derived from Transmembrane Protein 45A[1,2]

Esak Lee[*,†], Jacob E. Koskimaki[*], Niranjan B. Pandey[*] and Aleksander S. Popel[*,†,‡]

*Department of Biomedical Engineering, Johns Hopkins University School of Medicine, Baltimore, MD; †Department of Chemical and Biomolecular Engineering, School of Engineering, Johns Hopkins University, Baltimore, MD; ‡Department of Oncology and the Sidney Kimmel Comprehensive Cancer Center, Johns Hopkins University School of Medicine, Baltimore, MD

Abstract

Angiogenesis, the formation of new blood vessels from preexisting blood vessels, is a process that supports tumor growth and metastatic dissemination. Lymphangiogenesis also facilitates metastasis by increasing dissemination through the lymphatic vessels (LVs). Even after treatment with antiangiogenic agents, breast cancer patients are vulnerable to LV-mediated metastasis. We report that a 14–amino acid peptide derived from transmembrane protein 45A shows multimodal inhibition of lymphangiogenesis and angiogenesis in breast cancer. The peptide blocks lymphangiogenic and angiogenic phenotypes of lymphatic and blood endothelial cells induced by tumor-conditioned media prepared from MDA-MB-231 breast cancer cells. The peptide delays growth of MDA-MB-231 tumor xenografts and normalizes tumor-conditioned lymph nodes (LNs). These studies demonstrate the antilymphangiogenic and antiangiogenic potential of the peptide against primary tumors and premetastatic, tumor-conditioned regional LNs. Mechanistically, the peptide blocks vascular endothelial growth factor receptors 2 and 3 (VEGFR2/3) and downstream proteins by binding to neuropilin 1/2 (NRP1/2) and inhibiting VEGFR2/3 and NRP1/2 complex formation in the presence of VEGFA/C.

Neoplasia (2013) 15, 112–124

Introduction

Angiogenesis is a process that tumors employ to promote their growth and spread [1]. Although blood vessels contribute to cancer cell dissemination, tumor metastasis is significantly facilitated by the lymphatic system as well [2]. Studies in micrometastases of melanoma, gastric cancer, and breast cancer have shown that 16% to 20% of cancer patients showed lymphatic invasion, whereas 3% to 5.4% showed blood vessel invasion, bypassing the lymphatic system [3–5]. Lymphatic vessels (LVs) offer several advantages over blood vessels for cancer cell dissemination. The LVs have a discontinuous basement membrane that facilitates intravasation and extravasation of cancer cells. The LVs have a much slower flow rate of lymphatic fluid with lower shear stress, resulting in less tumor cell death, and a higher lymphatic concentration of hyaluronic acid, a molecule with potent cancer cell–protecting properties [6].

Metastasis is significantly enhanced by an increase in lymphangiogenesis in primary tumors and regional lymph nodes (LNs): These

pathologic phenomena at the two different sites are referred to as tumor lymphangiogenesis and LN lymphangiogenesis [7]. In terms of tumor lymphangiogenesis, peritumoral or intratumoral LVs play a role as initial routes of cancer cell dissemination from the primary tumor to the lymphatic system. LN lymphangiogenesis is also central for lymphatic metastasis; as shown, premetastatic or postmetastatic LNs feature highly enhanced lymphangiogenesis [8]. Before invasion, primary tumors overexpress lymphangiogenic factors and deliver these factors to tumor-draining LNs through LVs, thus inducing neolymphangiogenesis in the LNs [9]. Additionally, the LN lymphangiogenesis is maintained and further enhanced after cancer cells metastasize to the LNs [10]. These suggest that tumor lymphangiogenesis and LN lymphangiogenesis would be crucial targets of antimetastatic agents.

Breast cancer is the most commonly diagnosed female malignancy in the United States [11]. Though antiangiogenic or hormonal therapies combined with other agents are in development to treat breast cancer [12], many patients with metastatic breast cancer (e.g., triple-negative breast cancer subtypes) have suffered from recurrence of secondary tumors in regional LNs and distant organs [13,14]. Avastin (bevacizumab), a vascular endothelial growth factor A (VEGFA) monoclonal antibody, was revoked by the Food and Drug Administration from clinical indications for advanced breast cancer, because it had not improved overall survival rates of metastatic breast cancer patients [15]. This limitation of Avastin can be interpreted on the basis of the evidence that antiangiogenic therapies result in a hypoxic condition in tumors, overexpression of lymphangiogenic factors, enhancing tumor metastasis through the lymphatics [16,17]. Thus, lymphatic metastasis is an alternative way of tumor resistance to current antiangiogenic therapies.

Previously, our bioinformatics approach using peptides known to have antiangiogenic activity as the input resulted in the identification of more than 100 novel antiangiogenic endogenous peptides in the human proteome. These peptides are parts of larger proteins of different classes, including type IV collagen, thrombospondin-1, CXC chemokines, serpins, and somatotropins [18]. We recently discovered that small peptides from somatotropin domain–containing proteins are antilymphangiogenic and antiangiogenic in cell-based experiments [19]. On the basis of these findings, here we investigate the *in vivo* activity of one of the most potent somatotropin peptides, derived from a transmembrane protein 45A that we denote SP5031 (amino acid sequence: LLRSSLILLQGSWF-NH$_2$) in breast cancer models, including primary tumor xenografts and tumor-conditioned regional LNs, and investigate its mechanisms of action.

Materials and Methods

Peptide Synthesis and Handling

Peptides were produced by Bachem (Torrance, CA) by using a solid-phase synthesis technique. High-performance liquid chromatography (HPLC) and mass spectrometry (MS) analyses of the peptides were provided by the manufacturer to indicate a purity of more than 95%. In preparation of peptide stock solution, DMSO was used as a solvent at a maximum concentration of 5% (vol/vol) in distilled water. We verified that all experiments were carried out with <0.3% concentrations of DMSO so as not to harm cells. Theoretical isoelectric points of the peptides were calculated, using the Compute pI/Mw online software in ExPASy provided by the Swiss Institute of Bioinformatics (Lausanne, Switzerland).

Cell Culture

Lymphatic endothelial cells (LECs), microvascular endothelial cells (MECs), and human umbilical vein endothelial cells (HUVECs) were purchased from Lonza (Walkersville, MD). LECs and MECs were propagated in microvascular endothelial cell growth medium-2 (EGM-2MV; Lonza). HUVECs was propagated in endothelial cell growth medium-2 (EGM-2, Lonza). MDA-MB-231 triple-negative human breast cancer cells and MCF-7 estrogen receptor–positive human breast cancer cells were supplied by Dr Zaver Bhujwalla (Departments of Radiology and Oncology, Johns Hopkins Medical Institutions) and propagated in RPMI 1640 medium (Gibco, Carlsbad, CA) supplemented with 10% FBS (Gibco) and 1% penicillin-streptomycin (Gibco). Cells were maintained under standard conditions of 37°C and 5% CO$_2$ and the passage numbers of endothelial cells were kept between 3 and 6.

Preparation and Characterization of Tumor-Conditioned Media

MDA-MB-231 cells in complete growth media (RPMI 1640) were plated onto 175-mm^2 tissue culture plates. When the cell number reached 10×10^6 (confluent monolayer), the complete media were removed, and the cells were carefully rinsed with serum-free media (SFM; RPMI 1640 without supplements), and then, 5 ml of SFM was added. After 24 hours of incubation at 37°C, tumor-conditioned media (TCM) were carefully gathered, centrifuged, and filtered through 0.2-μm sterile syringe filters (Corning, Tewksbury, MA) to remove cells. The TCM was stored in aliquots at –80°C to avoid multiple freeze-thaws.

A Proteome Profiler Antibody Arrays Kit for Human Angiogenesis (R&D Systems, Minneapolis, MN) was used to determine angiogenesis-related factors in TCM. Array membranes were blocked with 2 ml of blocking buffer provided in the kit for 1 hour at room temperature on a rocking platform. One thousand microliters of TCM was mixed with 500 μl of dilution buffer provided in the kit. The prepared sample was added to the blocked membrane and the membrane was incubated overnight at 4°C. After three rinses with washing buffer provided in the kit, 1.5 ml of HRP-conjugated detection antibody in the kit was added for signal detection.

Migration and Adhesion Assays

Cell migration and adhesion assays were performed using Real-Time Cell Analysis (RTCA) System (ACEA Biosciences, San Diego, CA), as described previously [19]. To evaluate cell migration, we used Cell Invasion and Migration plates (CIM-plates; Roche, Indianapolis, IN) and an RTCA System. The membrane of the top chamber of a CIM-plate was precoated with 20 μg/ml fibronectin (Sigma-Aldrich, St Louis, MO). One hundred eighty microliters of TCM was added to the bottom chamber as a chemoattractant. Cells (45,000 HUVECs; 120,000 LECs/well) were added to the top chamber with or without peptides. After stabilizing CIM-plates for 30 minutes at room temperature, the chamber was loaded in the RTCA machine, and the cell indices were measured continuously for 24 hours. Cell indices at 20 hours were selected for analysis. For adhesion assays, 100 μl of 2× concentrated peptide solution was added to the appropriate wells of an E-plate (Roche). LECs and HUVECs (25,000 cells/well) in TCM were added next to each well, diluting peptides to the appropriate final concentration. After equilibrating at room temperature for 30 minutes, the E-plate was loaded into the RTCA System. Cell indices at 3 hours were analyzed.

Tube Formation Assay

Fifty microliters of Matrigel (BD Biosciences, Bedford, MA) was loaded in each well of a 96-well plate, and the plate was incubated at 37°C for 30 minutes. One hundred microliters of LECs and HUVECs in TCM with or without peptides were added on top of the matrix in the 96-well plate (15,000 cells/well). The plate was then incubated at 37°C, and the wells were imaged using a Nikon microscope at 20 hours (Nikon Instruments Inc, Melville, NY). Quantification of tube formation was assisted by S.CORE, a web-based image analysis system (S.CO Life Science, Munich, Germany). Tube formation indices represent the degree of tube formation. The indices were calculated using the equation below. The values of the variables used in the equation below were obtained automatically by S.CORE.

$$\text{(Tube formation index)} = (\text{mean single tube index})^2 \times (1 - \text{confluent area})$$
$$\times (\text{number of branching points} / \text{total length skeleton}).$$

Cell Proliferation Assay

Cell proliferation assay was carried out by using cell proliferation reagent WST-1 (Roche), as described previously [19]. For the proliferation assay, 2000 cells were plated onto a 96-well plate and allowed to attach for 4 hours, and the media were replaced with media with peptides. After 72 hours at 37°C, the number of viable cells was measured after adding WST-1, a reagent that is converted to a formazan whose absorbance at 450 nm is measured in a plate reader.

Oris Cell Migration Assay

Motility of MDA-MB-231 and MCF-7 cells was assessed by using the Oris Pro Cell Migration Assay Kit with fibronectin precoated plates (Platypus Technology, Madison, WI). Fifty thousand cancer cells in complete media (RPMI 1640, 10% FBS) were added to each well (100 μl/well) of the 96-well plate containing stoppers to prevent the cells from settling in the center region of the wells. Cells were allowed to adhere for 8 hours, after which the stoppers were carefully removed. After one rinse with SFM, 100 μl of complete media (10% or 25% FBS) with or without the peptide was added. After 18 hours, the cells were labeled with CellTracker Green (Invitrogen, Carlsbad, CA), according to the manufacturer's protocol. The cells that migrated to the center of the well were quantified by reading fluorescence at 485/530 nm on a Victor V plate reader (PerkinElmer, Salem, MA) and imaged using a fluorescence microscope (Eclipse T-100; Nikon, Brighton, MI). A detection mask was applied to the bottom of the plate to observe only the cells that migrated into the previously restricted region by obstructing the other parts of the well.

MCF-7 Cell Adhesion Assay

MCF-7 cells were prelabeled with CellTracker Green (Invitrogen) according to the manufacturer's protocol. While cells were being labeled, a 96-well plate was coated with 20 μg/ml fibronectin for 30 minutes at 37°C. Labeled cells in 25% FBS complete media were plated at a density of 10,000 cells/well in the 96-well plate with or without SP5031. After 3 hours, cells were washed three times with Dulbecco phosphate-buffered saline (DPBS) (with Ca^{2+}, Mg^{2+}) after which the fluorescence intensity was measured using the Victor V

plate reader. For the negative control, cell adhesion after 0 hour of cell/peptide treatment was observed.

In Vivo MDA-MB-231 Xenograft Models

Animal protocols were approved by the Institutional Care and Use Committee at the Johns Hopkins Medical Institutions. MDA-MB-231 cells (2×10^6) were orthotopically inoculated into the lower thoracic mammary fat pad of severe combined immunodeficient mice under anesthesia [50 mg/kg ketamine + 5 mg/kg acepromazine in phosphate-buffered saline (PBS)], and the tumors were allowed to grow until they reached around 100 mm^3. Peptide solution in PBS (15 mg/kg) or PBS (vehicle) was injected intraperitoneally (i.p.) and continued for 27 days. The tumor size was measured and the volume was calculated as previously described [20], using the formula: $V = 0.52 \times a \times b^2$, where a is the long axis and b is the short axis of the tumor. Each group has 8 to 10 mice.

In Vivo Tumor-Conditioned Regional LN Models

Fifty microliters of MDA-MB-231 TCM or SFM was subcutaneously administered through the scruff of athymic nude mice. These animals were either treated with SP5031 or with the vehicle (PBS; i.p. administration, 15 mg/kg) for 14 days. After 14 days, animals were killed; the axillary and brachial LNs were excised and the LN volumes were measured. The LN volumes (V) were calculated according to the formula: $V = 0.52 \times a \times b^2$, where a is the long axis and b is the short axis of the LN. The LNs were rinsed in PBS and fixed in 4% formalin for 16 hours for immunohistochemistry. Each group has four mice, giving 16 regional LNs (eight axillary LNs + eight brachial LNs) per experimental group.

Matrigel Plug Assay

Growth factor reduced Matrigel (High Concentration; BD Biosciences) containing rh-VEGF$_{165}$ (380 ng/ml; R&D Systems), recombinant human fibroblast growth factor-basic (rh-bFGF) (380 ng/ml; R&D Systems), and heparin (10 IU/plug; Sigma-Aldrich) was mixed with or without the peptide (200 μg/ml) in a total volume of 400 μl. The Matrigel mixtures were subcutaneously injected on both flanks on the abdominal side of athymic nude mice under anesthesia. After 10 days, the gels were removed, imaged, and analyzed by immunohistochemistry.

Immunohistochemistry

Axillary and brachial LNs fixed in 4% formalin were placed in 30% sucrose solution in PBS, incubated overnight at 4°C, and frozen in the Tissue-Tek Optimal Cutting Temperature compound (Sakura, Tokyo, Japan). Serial sections of 10-μm thickness were cut parallel to the long axis of the LN at –20°C. After blocking with 5% normal chicken serum in PBST (5% chicken serum, 0.1% cold fish gelatin, 0.1% Triton X-100, 0.05% Tween 20, and 0.05% sodium azide in PBS) for 1 hour at room temperature, the sections were treated with rat monoclonal anti-mouse MECA-79 antibody (Santa Cruz Biotechnology, Inc, Santa Cruz, CA) overnight at 4°C. After three rinses with PBST, sections were incubated with Alexa Fluor 647 chicken anti-rat IgG in the dark (Invitrogen) for 1 hour at room temperature. After three rinses, the second blocking agent (5% normal donkey serum in PBST) was added and incubation at room temperature in the dark was continued for another hour. Goat polyclonal anti-mouse LYVE-1 antibody was added and incubation was continued overnight after switching to 4°C, and Alexa Fluor 488 donkey anti-goat IgG (Invitrogen) was added and processed as above. The samples were

mounted with the ProLong Gold anti-fade reagent (Invitrogen). Matrigel plugs and breast tumor tissues were fixed in 4% formalin fixative solution for 16 hours and sent to a commercial vendor (Covance Inc, Princeton, NJ) to probe with CD34 and LYVE-1 antibodies, assessing blood vessels and LVs. We quantified MECA-79, CD34, and LYVE-1 using the FRiDA software (Johns Hopkins University, Baltimore, MD) and ImageJ (National Institutes of Health, Bethesda, MD), measuring the pixel intensity/4× frame of randomly selected 12 images in each group. Images shown are magnified to ×10 or ×20 to visually show greater surface area, and the fluorescent images from the LNs were merged, using the ImageJ software.

Histopathology

We performed hematoxylin and eosin (H&E) staining on lungs, liver, spleen, and kidney of animals that are treated with vehicle (PBS) or SP5031 for 27 days, assessing peptide toxicity in the animals. Lungs, liver, spleen, and kidney were harvested, rinsed with DPBS, and fixed in 4% formalin for 16 hours at room temperature. The organs were placed in 30% sucrose solution in DPBS, incubated overnight at 4°C, and frozen in the Tissue-Tek Optimal Cutting Temperature compound. Sections of 10-μm thickness were cut at –20°C. The sections were rehydrated in PBS for 5 minutes (×3) and immersed in the filtered 0.1% Mayer's hematoxylin solution (Sigma-Aldrich) for 10 minutes. Then, the slides were rinsed with tap water for 5 minutes. Next, the stained sections were co-stained with eosin by immersing the slides in 0.5% eosin Y solution (Sigma-Aldrich) for 1 minute. The slides were dipped in distilled water 10 times (×10). The sections were dehydrated in ascending ethanol (EtOH) solutions: 50% EtOH × 10 dips, 70% EtOH × 10 dips, 30-second incubation in 95% EtOH, and 1-minute incubation in 100% EtOH. The slides were rinsed with xylene two times. The slide was mounted with mounting media (50% glycerin) and covered with a slide glass. The slides were observed by using Olympus BX51TF with DP70 color camera (Olympus, Center Valley, PA).

Phospho–Receptor Tyrosine Kinase Proteome Analysis

A Proteome Profiler Antibody Arrays Kit for human phospho–receptor tyrosine kinase (p-RTK; R&D Systems) was used to determine which of the RTKs that are phosphorylated in the presence of TCM phosphorylation were inhibited by SP5031. Briefly, 2×10^6 LECs treated with or without 50 μM SP5031 for 90 minutes were stimulated by TCM (3× concentrated) for 10 minutes at 37°C. To prepare the concentrated TCM (3×), we used 3.6 ml of RPMI SFM and 20×10^6 cancer cells in plates: Other conditions were the same as the protocol for preparation of TCM described above. Treatments were stopped by adding cold PBS; the cells were lysed in cold lysis buffer [150 mM NaCl, 1 mM EDTA, 100 μl/ml protease inhibitors (Sigma-Aldrich), 10 μl/ml phosphatase inhibitors (Sigma, St Louis, MO), and 1% Triton X-100] for 2 hours at 4°C and then scraped to collect the lysates. Cell lysates were spun at 14,000g for 15 minutes to remove cell debris. Array membranes were blocked with blocking buffer provided in the kit. Cell lysate was mixed with dilution buffer, the prepared sample was added to the blocked membrane, and the membrane was incubated overnight at 4°C. After three rinses, anti–phospho-tyrosine-HRP detection antibody (diluted by 1:2000 with dilution buffer in the kit) was added, and the antibody-bound streptavidin-HRP complex was detected by using a chemiluminescence detection reagent (GE Healthcare, United Kingdom).

Western Blot Assay

HUVECs, MECs, and LECs were grown in complete growth media and plated onto tissue culture–treated six-well plates at 400,000 cells/well in complete media (CM). Cells were starved in SFM for 24 hours after which SP5031 was added for 90 minutes. VEGFA (20 ng/ml) or VEGFC (100 ng/ml) was added, and the incubation was continued for 10 minutes at 37°C. Treatments were stopped by adding cold PBS, and cell lysates were prepared as described above. Cell lysates were separated by sodium dodecyl sulfate–polyacrylamide gel electrophoresis (SDS-PAGE) and transferred to nitrocellulose blots (Invitrogen). We blocked for 1 hour with 5% nonfat milk + 1% BSA in tris-buffered saline and tween 20 (TBST) and probed with antibodies of interest including phosphorylated VEGF receptor 2 (VEGFR2; Y1175), VEGFR2, phospho-mitogen-associated protein kinase kinase 3/6 (pMKK3/6; S189/S207), phospho-p38 mitogen-associated protein kinase (pp38MAPK; T180/Y182), MAP kinase-activated protein kinase 2 (p-MAPKAPK2; T334), phosphorylated heat shock protein 27 (HSP27; S82), phospho-Src (pSrc; Y416), Src, glyceraldehyde 3-phosphate dehydrogenase (GAPDH; Cell Signaling Technology, Inc, Danvers, MA), and 4G10 pan-tyrosine phosphorylation antibody (Santa Cruz Biotechnology, Inc). GAPDH was used as a loading control. Secondary antibodies were added at 1:2000 dilution and protein bands detected with a chemiluminescence detection reagent (GE Healthcare).

Sulfo-SBED Cross-Linking Assay

We used a cross-linking strategy with Sulfo-SBED cross-linking reagent to identify target receptors of SP5031 on blood endothelial cells (BECs) and LECs. A Sulfo-SBED Biotin Label Transfer Reagent (Thermo Scientific Inc, Rockford, IL) has three functional groups, including an amine-reactive N-hydroxysuccinimide (NHS)-ester group, a UV-activatable aryl azide group, and a biotin group. The peptide was reacted with Sulfo-SBED at ratio of 1:3 in PBS at room temperature for 2 hours, in the dark. After the reaction, unreacted Sulfo-SBED was quenched with excess Tris-HCl. HUVECs or LECs were rapidly gathered from cell culture plates, using a nonenzymatic cell dissociation reagent (Sigma-Aldrich) and rinsed with PBS to remove serum proteins on the cell surface. Probe-conjugated peptide (15 μM; 30 μl) was added to 1×10^7 HUVECs or LECs in 1 ml of PBS in a 24-well plate, and the mixture was incubated at room temperature for 1 hour on a rocker. The 24-well plate was exposed in UV (365 nm) without a lid for 15 minutes. UV-exposed cells were rinsed with 1 ml of cold PBS twice (centrifuged at 3000 rpm, 4°C for 5 minutes) to remove unreacted probes and dead cells. The rinsed cells were resuspended in 500 μl of cell lysis buffer and incubated in an ice bath for 1 hour, with vortexing every 20 minutes. Fifteen microliters of streptavidin sepharose bead (Cell Signaling Technology, Inc) was added in the cell lysates, and the mixture was incubated at 4°C for 2 hours. The beads were rinsed three times with 500 μl of lysis buffer. The beads were collected by a brief spin in a microfuge tube. The collected beads were boiled for 10 minutes with sample reducing buffer (4×). The reduced sample was centrifuged at 14,000g for 15 minutes, and the supernatant was separated by SDS-PAGE and probed with anti-biotin, anti–neuropilin 1 (NRP1), anti-NRP2, anti-CD44, anti-VEGFR2, and anti-VEGFR3 (Cell Signaling Technology, Inc). For competition assays, we added 10× molar excess of unlabeled SP5031 or 10× unlabeled SP5002 in the wells containing LECs/BECs and the SP5031 probe. After the same cross-linking process as above, LEC or BEC cell lysates were immunoprecipitated with anti-NRP1 or anti-NRP2 (Cell Signaling Technology, Inc) antibodies plus Protein A/G Plus Agarose (Santa Cruz Biotechnology, Inc) as

above; the immunoprecipitated proteins were separated and probed with anti-biotin (HRP-linked) antibodies.

Co-immunoprecipitation

Co-immunoprecipitation (co-IP) was performed to investigate molecular interaction between NRP1 and VEGFR2 in HUVECs or between NRP2 and VEGFR3 in LECs. To optimize conditions for co-IP, we tested cell lysis buffers with different ionic strengths and detergents (50, 100, and 150 mM NaCl; 0.1% and 1% Triton X-100) in VEGFA-induced VEGFR2-NRP1 complex formation in HUVEC lysates. To determine SP5031 activity, we treated 4×10^6 HUVECs or 1.2×10^7 LECs with SP5031 for 90 minutes followed by induction with VEGFA (40 ng/ml) or VEGFC (100 ng/ml). Optimized cell lysis buffer [50 mM NaCl, 20 mM Tris-HCl, 1 mM EDTA, 100 µl/ml protease inhibitors (Sigma), 10 µl/ml phosphatase inhibitors (Sigma), and 1% Triton X-100 (Sigma)] was used to conserve the receptor complex. Five hundred microliters of cell lysates was incubated overnight at 4°C with antibodies suitable for IP: rabbit anti-VEGFR2 antibody; rabbit anti-NRP1 antibody; rabbit anti-NRP2 antibody (Cell Signaling Technology, Inc); mouse anti-VEGFR3 (EMD Millipore, Billerica, MA). Protein A/G Plus Agarose (Santa Cruz Biotechnology, Inc) was added and the tubes rocked for 3 hours at 4°C. The beads were rinsed three times with 500 µl of cell lysis buffer, and the protein complex was reduced and separated by SDS-PAGE and probed with the following antibodies: mouse anti-NRP1, mouse anti-VEGFR2 (R&D Systems), mouse anti-NRP2, rabbit anti-NRP2, rabbit anti-VEGFR3 (Cell Signaling Technology, Inc), and mouse anti-VEGFR3 (EMD Millipore).

Statistical Analysis

Error bars correspond to SEM, unless otherwise stated. Differences between a control and a peptide-treated group are regarded as significant when P is less than .05 using the Student's t test.

Results

SP5031 Blocks Migration, Adhesion, and Tube Formation of LECs and BECs in TCM

The RTCA System was used to measure TCM-induced migration and adhesion of LECs and BECs with or without SP5031. SP5031 peptide significantly inhibited TCM-induced migration of LECs and BECs. TCM contains multiple angiogenesis-related factors as will be presented below. SP5031 (50 µM) inhibited LEC migration by 83.5% ($P < .01$) and BEC migration by 56.0% from control (Figure 1, *B* and *C*). SP5031 also inhibited LEC adhesion (30.0% inhibition
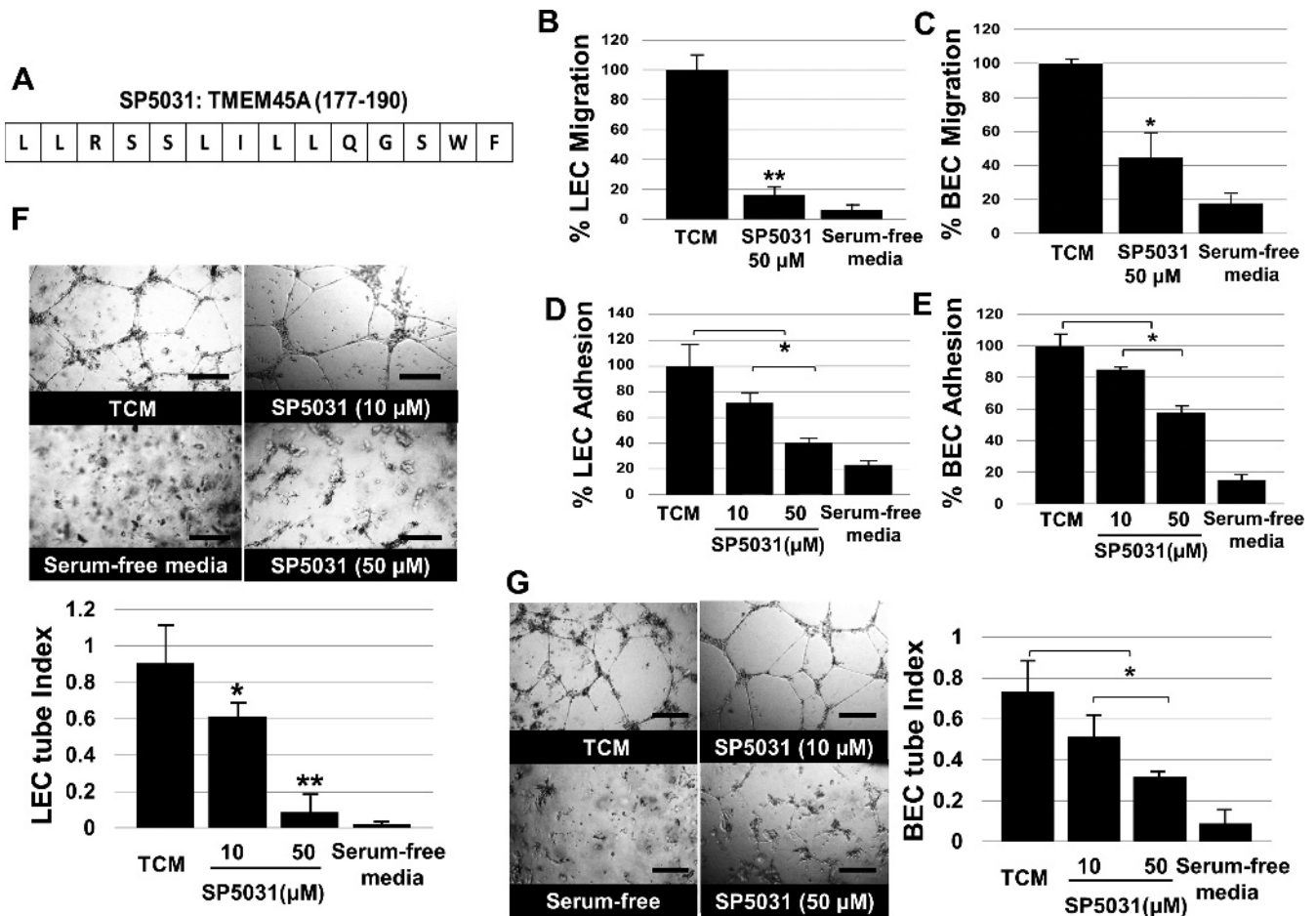

Figure 1. *In vitro* activity of SP5031 on LECs and BECs. (A) Amino acid sequence of the SP5031 peptide. (B) Percent LEC migration at 20 hours. **P < .01 *versus* TCM-treated control. (C) Percent BEC migration (*P < .05). (D) Percent LEC adhesion (*P < .05). (E) Percent BEC adhesion (*P < .05). (F) SP5031 inhibits TCM-induced LEC tube formation. LEC tube index (S.CORE quantification) shows dose response of SP5031 (*P < .05 and **P < .01). S.CORE (S.CO Life Science) is a web-based image analysis system [19]. Scale bars represent 200 *µ*m. (G) BEC tube formation (*P < .05). Scale bars represent 200 *µ*m.
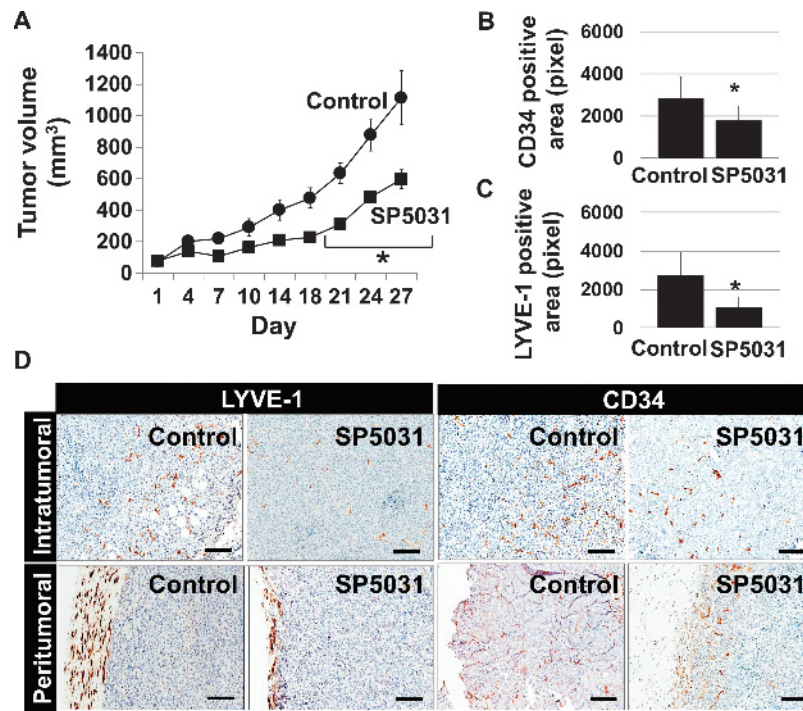
Figure 2. MDA-MB-231 xenografts with SP5031 treatment. SP5031 blocks lymphangiogenesis and angiogenesis in MDA-MB-231 xenografts. (A) Changes in tumor volume of the PBS or SP5031-treated groups. After day 21, SP5031 significantly delayed tumor growth compared to control (*$P < .05$). (B) Quantification of blood vessels in the tumors (*$P < .05$). (C) Quantification of LVs (*$P < .05$). (D) Representative immunohistochemistry images from intratumoral and peritumoral regions of the tumor. Scale bars represent 100 μm.

with 10 μM SP5031; 61.0% inhibition with 50 μM SP5031) and BEC adhesion (17.2% inhibition with 10 μM SP5031; 42.4% inhibition with 50 μM SP5031; Figure 1, *D* and *E*). The original data for LEC/BEC migration and adhesion are shown in Figure W1. SP5031 limited TCM-induced LEC tube formation (33.5% inhibition with 10 μM SP5031; 93.0% inhibition with 50 μM SP5031, $P < .01$) and also inhibited TCM-induced BEC tube formation (32.2% inhibition with 10 μM SP5031; 58.0% inhibition with 50 μM SP5031, $P < .05$; Figure 1, *F* and *G*).

SP5031 Exhibits Antilymphangiogenic and Antiangiogenic Activity in MDA-MB-231 Tumor Xenografts

We next tested the activity of SP5031 in an MDA-MB-231 orthotopic xenograft model. We showed that 15 mg/kg SP5031 administered i.p. daily delayed tumor growth compared to a PBS-treated control group. At the end of the experiment, the SP5031-treated group showed 51.0% less tumor growth than the control group ($P < .05$; Figure 2A). Immunostaining with mouse anti-CD34 and mouse anti–LYVE-1 demonstrated that SP5031 blocked formation of stromal blood and LVs in both intratumoral and peritumoral areas (Figure 2D). There were 35.7% fewer blood vessels and 62.0% fewer LVs ($P < .05$) in tumor tissues from animals treated with SP5031 (Figure 2, *B* and *C*).

SP5031 Blocks Migration of MDA-MB-231 and MCF-7 Breast Cancer Cells

We performed tumor cell migration assay using Platypus cell migration kits (Figure W7). Tumor cell migration is one of the standards to determine tumorigenic potential of the cancer cells. We treated MDA-MB-231 cells with SP5031 because we have observed that SP5031 delayed MDA-MB-231 tumor growth *in vivo*. We additionally assessed

SP5031 on MCF-7 breast cancer cells, an estrogen receptor–positive breast cancer cell line. Ten percent FBS induced significant migration of MDA-MB-231 cells ($P < .05$); however, MCF-7 did not migrate at that condition. At 25% FBS, MCF-7 showed significant migration ($P < .05$); thus, we tested SP5031 at 25% FBS in both cell lines (Figure W7, *A* and *C*). We showed the inhibition of tumor cell motility on both breast cancer cell types by treating with SP5031 (Figure W7, *B* and *D*). SP5031 potently inhibited MDA-MB-231 cell migration at 60 and 20 μM (68% and 44% inhibition) and MCF-7 migration at 60, 20, and 6.7 μM (74%, 70%, and 65% inhibition, respectively).

SP5031 Blocks Adhesion of MCF-7 Breast Cancer Cells

We performed adhesion assays using MCF-7 breast cancer cells. At 3 hours after cell seeding in 25% FBS, MCF-7 cells showed adhesion on a fibronectin-coated plate. Peptide-treated group showed significant inhibition of cell adhesion compared to control (Figure W8).

SP5031 Shows Antilymphangiogenic and Antiangiogenic Activity in Tumor-Conditioned Regional LNs

We developed a tumor-conditioned regional LN model by injecting TCM subcutaneously into animals for 14 days to simulate the conditioning of tumor-draining LNs by primary tumor–secreted factors that are transported to the LNs through LVs [10,21]. We found that the axillary and brachial LNs of TCM-treated animals were two to three times larger than those of SFM-treated animals. Next, we co-administered SP5031 in TCM-treated animals. The SP5031-treated group showed significant normalization of the LN volume ($P < .05$; Figure 3, *A* and *B*). Anti-mouse LYVE-1 and anti-mouse MECA-79 antibodies were used to detect LVs and high endothelial venules (LN-specific vascular endothelium) in the LNs. TCM treatment enhanced LV density

(LVD) by 87.7% in axillary LNs and by 66.0% in brachial LNs and blood vessel density (BVD) by 101.0% in axillary LNs and by 98.2% in brachial LNs. SP5031 normalized both TCM-enhanced LVD and BVD significantly ($P < .05$) (Figure 3, C and D). These results demonstrate that SP5031 blocks both LN lymphangiogenesis and LN angiogenesis in tumor-conditioned axillary and brachial LNs.

SP5031 Blocks TCM-Induced VEGFR2 Phosphorylation

The pro-angiogenic and pro-lymphangiogenic factors present in TCM were determined using Proteome Profiler Human Angiogenesis Array Kits. MDA-MB-231 cells expressed pro-angiogenic factors, including angiogenin, chemokine ligand 16, heparin-binding epidermal growth factor–like growth factor, matrix metalloproteinases 8 and 9, PDGF-AA, endothelin-1, interleukin 8, VEGFA, and placental growth factor. Interestingly, TCM contained antiangiogenic factors as well, including serpin E1, serpin F1, tissue inhibitor of metalloproteinase 1, and thrombospondin-1. However, a well-known lymphangiogenic factor, VEGFC, was not detected in TCM (Figure 4A). Two million LECs pretreated with or without 50 μM SP5031 were stimulated by TCM. Lysates from these LECs were analyzed
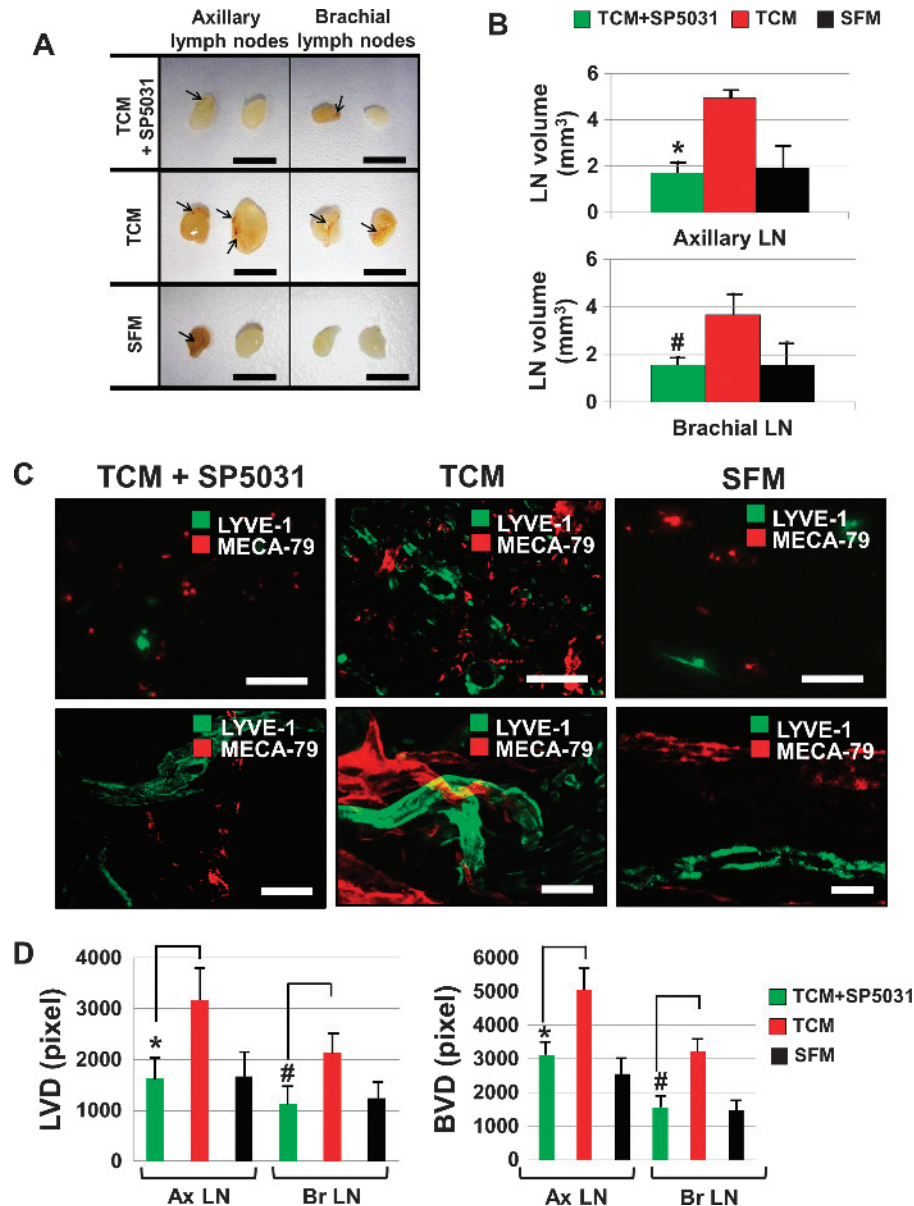

Figure 3. Tumor-conditioned regional LN models with SP5031 treatment. SP5031 inhibits lymphangiogenesis and angiogenesis in axillary and brachial LNs induced by TCM treatment. (A) Representative images of axillary and brachial LNs. Arrows represent macroscopically detectable blood vessels. Scale bars represent 3 mm. (B) LNs from TCM-treated mice show an increase in LN volumes. SP5031 treatment normalized the volume of the LNs. *$P < .05$ and #$P < .05$ *versus* the TCM-treated group. (C) Representative immunofluorescence images for LVs (green) and high endothelial venules [38]. Scale bars represent 100 μm. (D) Quantification of LVD and BVD in LNs. TCM enhances LVD by 87.7% in axillary LN (ax-LN) and by 66.0% in brachial LN (br-LN) and BVD by 101.0% in ax-LN and by 98.2% in br-LN. SP5031 treatment normalized the LVD and BVD in the LNs in TCM-treated animals significantly. *$P < .05$ (ax-LN), #$P < .05$ (br-LN) in LVD and *$P < .05$ (ax-LN), #$P < .05$ (br-LN) in BVD.
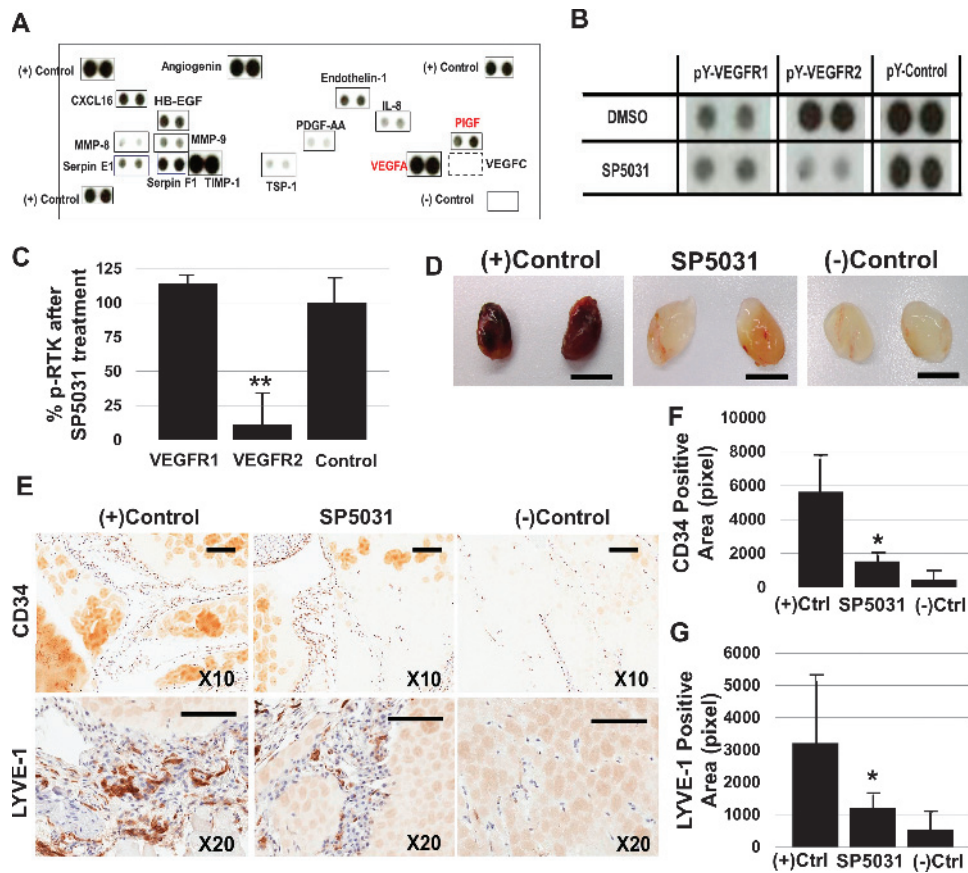
Figure 4. TCM-induced p-RTK analysis and VEGFA-induced Matrigel plug assays. (A) Angiogenesis factors in MDA-MB-231 TCM. (B) SP5031 (50 μM) inhibits phosphorylation of VEGFR2, not VEGFR1. (C) Percent p-RTK after treatment with SP5031, compared to control. SP5031 treatment lowers the phosphorylation of VEGFR2. **$P < .01$ *versus* control. (D) Representative Matrigel plugs with VEGFA plus or minus SP5031. Scale bars represent 10 mm. (E) Representative immunohistochemistry images from the Matrigel plugs. Images show that SP5031 treatment blocks VEGFA-induced angiogenesis (CD34) and lymphangiogenesis (LYVE-1) *in vivo*. Scale bars represent 100 μm. (F) Quantification of blood vessels in the plugs (*$P < .05$). (G) Quantification of LVs in the plugs (*$P < .05$).

by p-RTK Proteome Array Kits to determine the phosphorylation status of multiple RTKs. SP5031 specifically inhibited the phosphorylation of VEGFR2 by 87.0% compared to control; however, phosphorylation of VEGFR1 was not influenced by peptide treatment (Figure 4, *B* and *C*). Thus, the inhibition of VEGFR2 phosphorylation by SP5031 must be a result of activity against the VEGFA that is present in TCM (Figure 4*A*).

SP5031 Exhibits Antilymphangiogenic and Antiangiogenic Activity in Matrigel Plug Assays

Next, we implanted Matrigel plugs containing VEGFA with or without SP5031 into athymic nude mice (Figure 4*D*). We additionally included bFGF and heparin in the Matrigel plugs, because bFGF supports survival of endothelial cells and heparin enhances the interaction between VEGFA and VEGFR2. After 10 days, plugs containing VEGFA, bFGF, and heparin (positive control group) showed pronounced angiogenesis that SP5031 significantly inhibited: CD34-positive area was decreased by 74.0% compared to the growth factor–treated control group (Figure 4, *D* and *F*). LYVE-1, a marker for LVs was used to measure VEGFA-induced lymphangiogenesis in the plugs [22]. SP5031 inhibited LVs by 65.4% compared to the control (Figure 4, *E* and *G*). These results demonstrate that the antilymphangiogenic and antiangiogenic activities of SP5031 are achieved by targeting VEGFA in the plugs.

SP5031 Inhibits VEGFA/C-Dependent VEGFR2/3 Signals, Resulting in Inhibition of Activation of Downstream Proteins

Given the result that SP5031 blocks the phosphorylation of VEGFR2, we expanded our experiments to test for its effect on phosphorylation of VEGFR3 on LECs. VEGFR3, which is activated by VEGFC, is one of the major receptors for lymphangiogenic signaling on LECs. We tested SP5031 on LECs and BECs stimulated by VEGFC and VEGFA separately (Figure 5). As shown in Figures 5*A* and W2, SP5031 potently inhibited VEGFA-induced phosphorylation of VEGFR2, focal adhesion kinase (FAK), MKK3/6, p38MAPK, MAPKAPK2, and HSP27 in BECs (HUVECs and MECs). VEGFC-dependent phosphorylation of VEGFR3, VEGFR2, and FAK in LECs were also blocked by SP5031 (Figure 5*B*). This result was confirmed in a VEGFC-induced LEC migration assay in which 50 μM SP5031 inhibited LEC migration by 80.0% ($P < .05$; Figures 5*C* and W3). These results demonstrate that SP5031 inhibits the phosphorylation of VEGFR2, VEGFR3, and downstream proteins on LECs and BECs.

NRP1/2 Are the Target Receptors of SP5031

We used a cross-linking strategy to identify potential receptors of SP5031. SP5031 was conjugated to the trivalent Sulfo-SBED biotin-carrying reagent (Figure W4*A*). The conjugated SP5031–Sulfo-SBED (SP5031 probe) was applied to BECs or LECs followed by exposure to

UV light to allow cross-linking to occur (Figure W4*B*). Given that SP5031 inhibits VEGFR2 and VEGFR3 phosphorylation, we asked if target proteins could be NRP1, NRP2, CD44, VEGFR2, or VEGFR3 in immunoblot analysis experiments using the corresponding anti-

bodies. NRP1 and NRP2 were suspected because of their role as co-receptors of VEGFA and VEGFC in activation of VEGFR2 and VEGFR3, respectively [23,24]. CD44 was also suspected because of the role of CD44v3 and CD44v6 in endothelial cell migration and
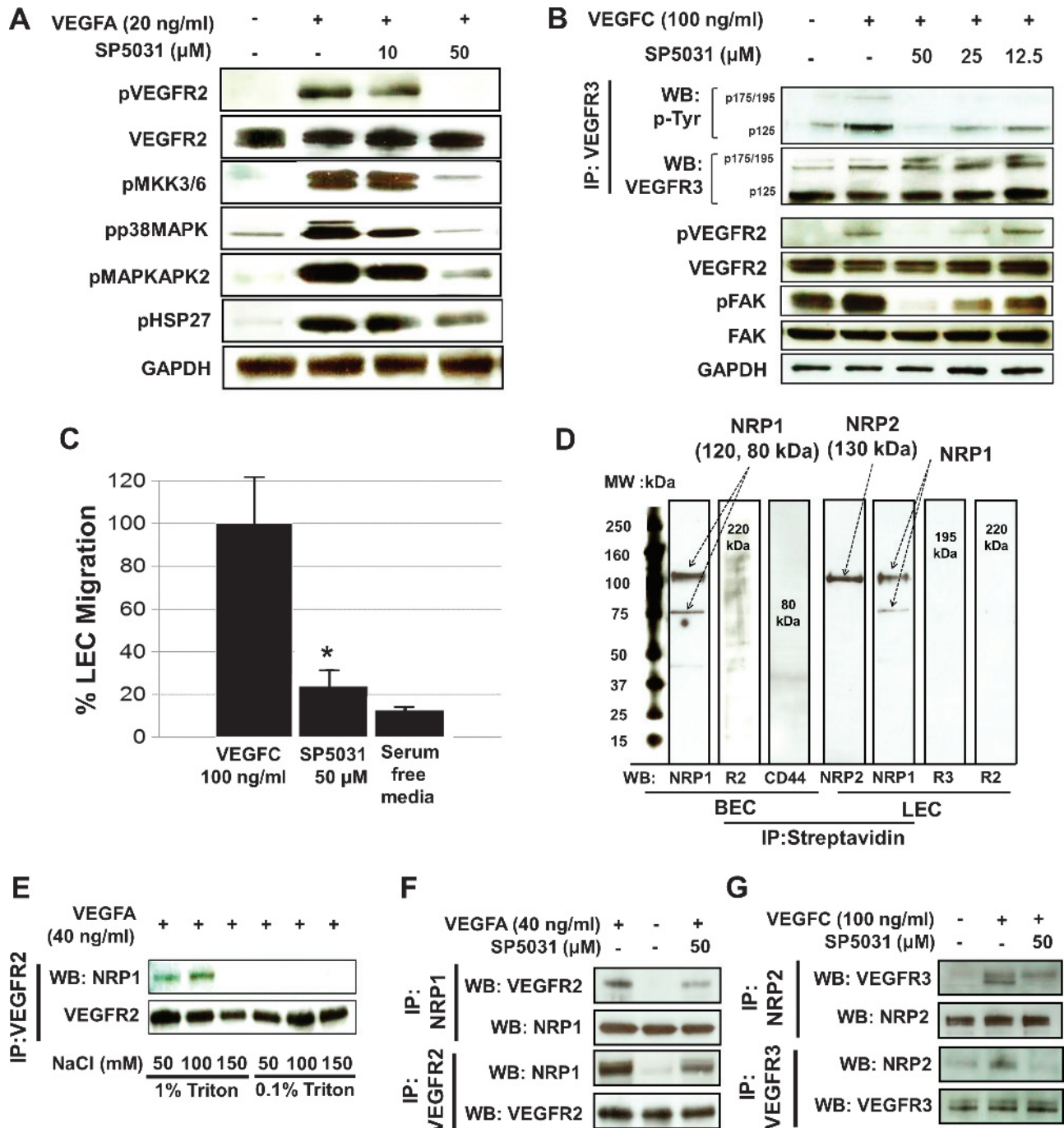

Figure 5. Inhibition of VEGFC and VEGFA signaling by SP5031 binding to NRP2 and NRP1. (A) SP5031 blocks VEGFA-induced phosphorylation of VEGFR2 (Y1175) and p38MAPK signaling proteins, including MKK3/6 (S189, S207), p38MAPK (T180, Y182), MAPKAPK2 (T334), and HSP27 (S82). (B) VEGFC-dependent phosphorylation of VEGFR3 (p-Tyr), VEGFR2 (Y1175), and FAK (4G10) were inhibited by SP5031 in LECs. GAPDH levels were used to control for the amount of total proteins in all cases. (C) VEGFC-induced LEC migration with or without SP5031 (*$P < .05$). (D) We identified target receptors of SP5031 by using a cross-linking strategy. Biotinylated (cross-linked) proteins are purified and probed using antibodies: The biotinylated target proteins were found to be NRP1 (80, 120 kDa) and NRP2 (130 kDa). (E) Co-IP assays were performed to optimize complex formation between VEGFR2 and NRP1 in the presence of VEGFA. (F) Treatment with SP5031 hindered VEGFA-induced complex formation between NRP1 and VEGFR2 in HUVECs. (G) Treatment with SP5031 blocked VEGFC-induced complex formation between NRP2 and VEGFR3 in LECs.
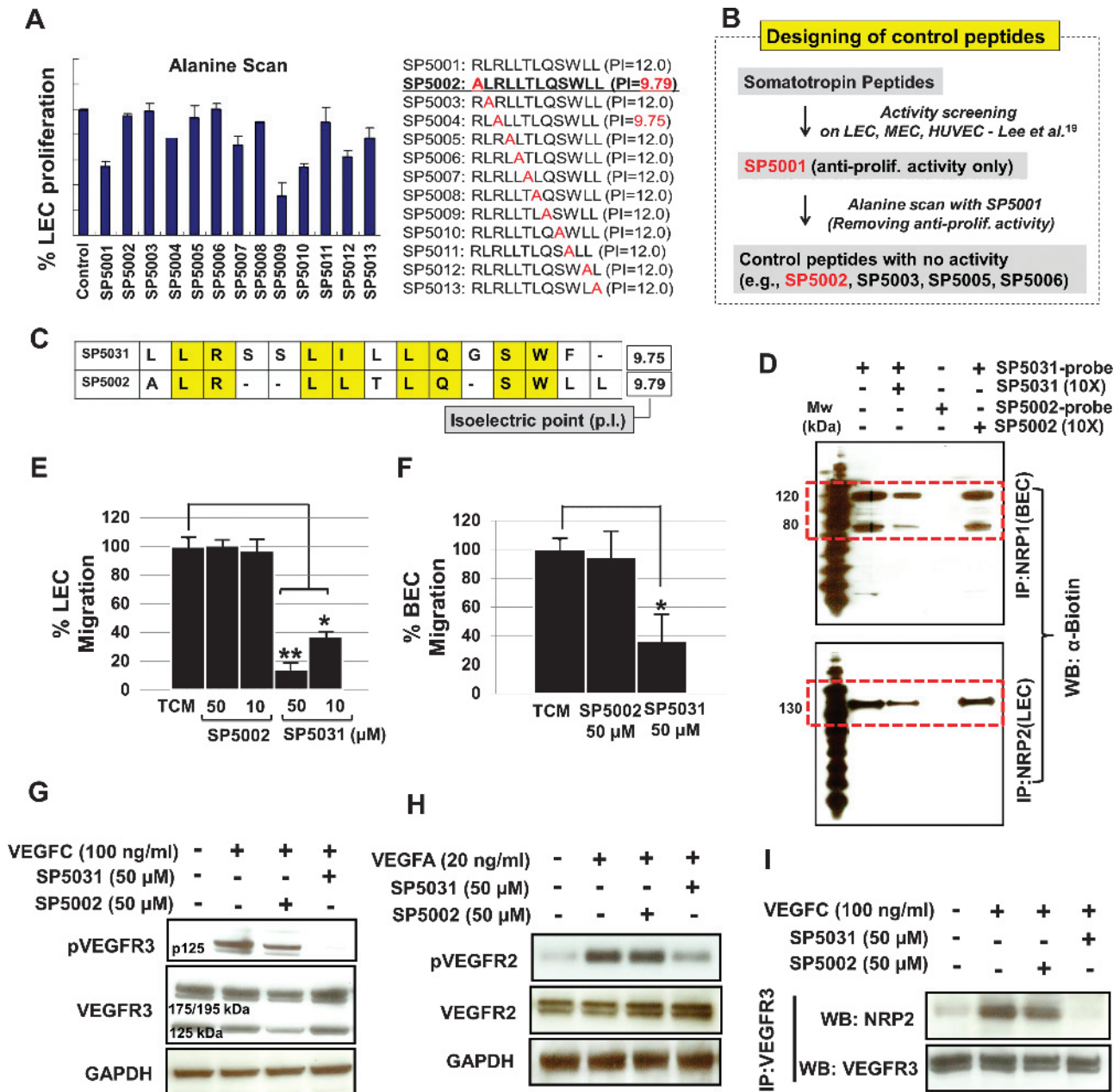
Figure 6. SP5031 binding to its receptors is specific. (A) Alanine scan of SP5001 to eliminate proliferation inhibitory activity of SP5001. (B) Flowchart for the identification of control peptides. (C) Peptide sequence comparison between SP5031 and SP5002. (D) SP5031 probe bound to NRP1 and NRP2 on BECs and LECs (lane 1). Competition with 10× unlabeled SP5031 lowered the amount of binding of SP5031 probe to its target receptors (lane 2). SP5002 probe did not bind to the same target receptors (lane 3). Competition with 10× unlabeled SP5002 did not hinder the binding of SP5031 probe to its target receptors (lane 4). (E) Percent LEC migration. SP5002 did not cause inhibition of LEC migration. However, SP5031 showed potent inhibition (*$P < .05$ and **$P < .01$). (F) Percent BEC migration (*$P < .05$). (G) VEGFC-induced phosphorylation of VEGFR3 was not significantly inhibited by SP5002 compared to SP5031. (H) VEGFA-induced phosphorylation of VEGFR2 was not inhibited by SP5002. (I) VEGFC-dependent complex formation between VEGFR3 and NRP2 was significantly dissociated by SP5031, however, not by SP5002.

adhesion through VEGFR2 signaling in the presence of VEGFA [25,26]. Surprisingly, we found that NRP1 and NRP2 but not CD44 and VEGFR2/3 cross-linked to SP5031 on LECs and BECs (Figure 5D). Next, we performed co-IP experiments with VEGFR2/3 and NRP1/2 antibodies in the presence of VEGFA/C with or without SP5031, as described previously [23]. We showed that upon activation with VEGFA, VEGFR2 and NRP1 formed a receptor complex (Figure 5E). SP5031 treatment hindered VEGFA-induced VEGFR2/

NRP1 complex formation in BECs, and VEGFC-induced VEGFR3 and NRP2 complex formation in LECs (Figure 5, F and G). However, VEGFR2 and CD44 complex formation in BECs was not inhibited by SP5031 treatment consistent with the finding that CD44 is not a target receptor of SP5031 (Figure W5). These results demonstrate that the peptide binding to NRP1/2 hinders receptor complex formation between VEGFR2/3 and NRP1/2, which results in suppression of VEGFA/C signal transduction.

SP5002, a Peptide Homologous to SP5031, Is Inactive

We generated a sham peptide, SP5002, which is homologous to wild-type SP5031 (Figure 6). In a previous screen of a number of somatotropin peptides on cell proliferation, migration, and adhesion of LECs, MECs, and HUVECs, we discovered that SP5001 (amino acid sequence: RLRLLTLQSWLL-NH$_2$) had antiproliferative but no antimigratory activity (Figure 6B) [19]. We performed an alanine scan of SP5001 to determine the amino acids that are crucial for its antiproliferative activity. We discovered that SP5002, SP5003,

SP5005, SP5006, and SP5011 did not inhibit LEC proliferation (Figure 6A). Among them, SP5002 has a nearly identical isoelectric point (of 9.75) to SP5031 (Figure 6C), suggesting that the overall surface charge and peptide solubility of SP5002 are comparable to those of SP5031 under the same experimental conditions. First, the effect of SP5002 and SP5031 on TCM-induced migration of LECs and BECs was evaluated. Even at 50 μM, SP5002 did not significantly inhibit migration of either cell type. SP5031 potently inhibited migration of both cell types under the same conditions
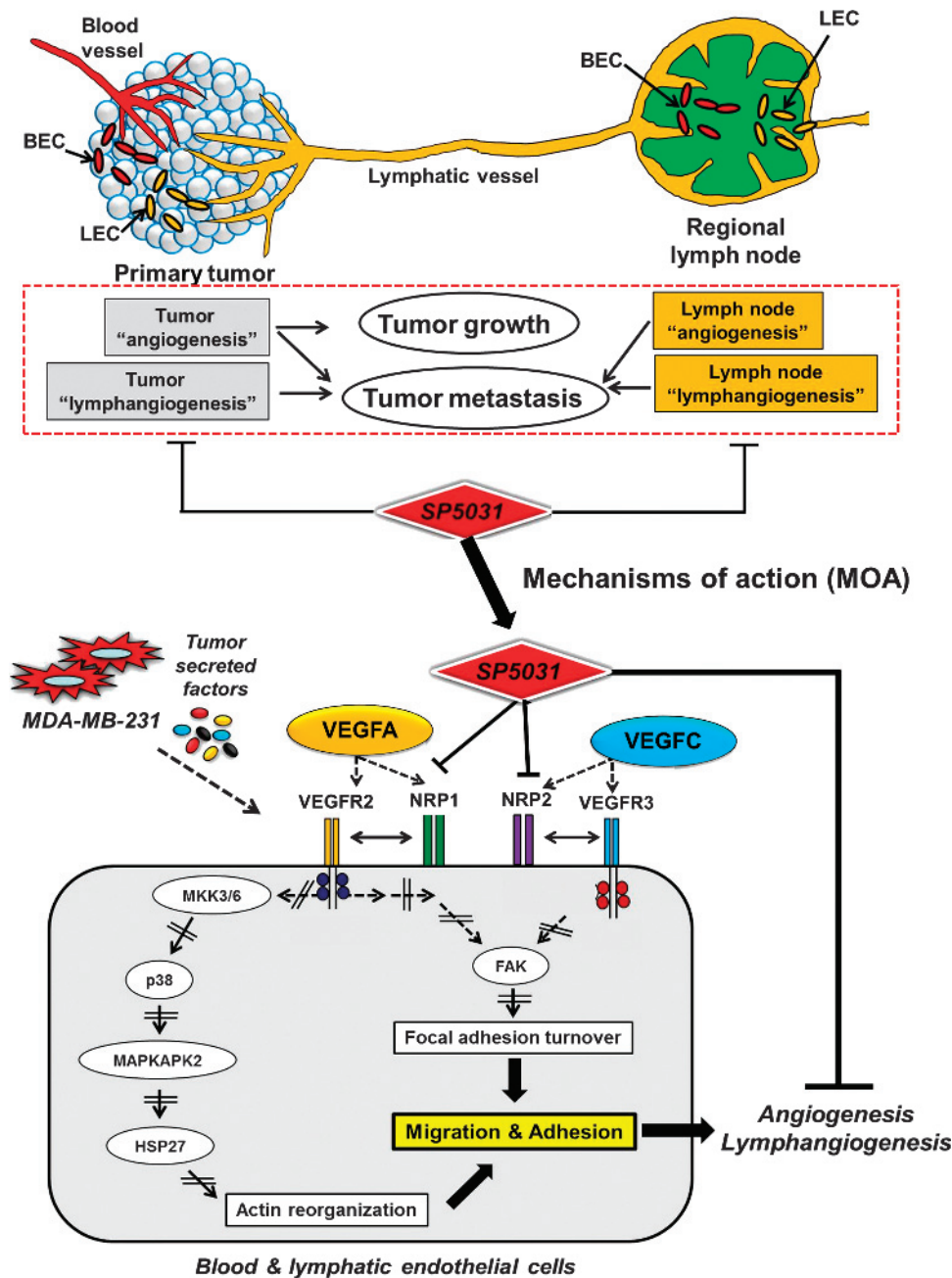

Figure 7. Mechanisms of action of SP5031. SP5031 inhibits lymphangiogenesis and angiogenesis in primary tumors and tumor-conditioned regional LNs. This suggests the potential of SP5031 to prevent both tumor growth and tumor metastasis (upper panel, hypothetical mechanisms are shown in a red dotted rectangle). At the cellular level, SP5031 targets LECs and BECs (lower panel). NRP1 (on BECs) and NRP2 (on LECs) are the target receptors. Peptide binding to NRP1 and NRP2 indirectly inhibits signaling from VEGFR2 and VEGFR3 in the presence of VEGFA and VEGFC. SP5031 further inhibits VEGF-induced phosphorylation of p38MAPK signaling molecules and FAK, element proteins for endothelial cell migration and adhesion.

(Figure 6, *E* and *F*). Next, SP5002 did not significantly inhibit VEGFA-induced phosphorylation of VEGFR2 on BECs and VEGFC-induced phosphorylation of VEGFR3 on LECs (Figure 6, *G* and *H*). SP5002 also did not hinder VEGFC-induced complex formation between VEGFR3 and NRP2 unlike SP5031 (Figure 6*I*). A cross-linking experiment in the presence of excess peptide as a competitor was performed with the SP5002 probe and the SP5031 probe (Figure 6*D*). SP5031 probe was efficiently cross-linked to NRP1 (120, 80 kDa) and NRP2 (130 kDa) on BECs and LECs (Figure 6*D*, lane 1). When unconjugated SP5031 at a 10-fold excess to SP5031 probe was included in the cross-linking assay, cross-linking of SP5031 probe to the target receptors was significantly reduced (Figure 6*D*, lane 2). These results demonstrate specific binding of SP5031 to these target receptors. SP5002 probe showed no binding to NRP1 and NRP2 in BECs and LECs (Figure 6*D*, lane 3). Very importantly in a competition assay, a 10-fold excess of SP5002 was not able to compete for binding to receptors of SP5031 (Figure 6*D*, lane 4). These results demonstrate that the activity of SP5031 is not because of nonspecific binding due to its overall surface charge but because of sequence specific interactions with the target receptors.

Discussion

Most malignant tumors exploit adaptive-evasive responses to the VEGF monoclonal antibody (bevacizumab) by switching their dependence to alternative pro-angiogenic signals and enhancement of distant metastasis mediated by lymphatics [13,16]. Sunitinib, a multitargeted tyrosine kinase inhibitor, however, exhibited antiangiogenic activity and allowed less lymphatic metastasis, as it targets both angiogenesis and lymphangiogenesis by inhibiting a large number of RTKs, including the VEGFRs and PDGF receptors [27]. In addition to those receptors, sunitinib blocks more than 70 tyrosine kinases with other activities, which are thought to lead to several side effects (e.g., hand-foot syndrome, stomatitis, hypothyroidism, and dermatologic toxicities) [28]. The two different examples discussed above (bevacizumab and sunitinib) suggest that single-target drugs are inadequate as therapeutics and also that agents that inhibit multiple common targets such as tyrosine kinases or G protein-coupled receptors (GPCRs) are problematic as effective therapeutics because of toxicity. However, we expect SP5031 to be an effective cancer therapeutic because it inhibits angiogenesis and lymphangiogenesis, two of the primary drivers of tumor growth and metastasis, highly specifically, thus we expect with minimal toxicity.

In terms of cytotoxicity of SP5031, we previously evaluated apoptotic and cytotoxic activities of SP5031, using caspase-3/7 and lactate dehydrogenase tests [19]. In this study, we showed no cytotoxicity or apoptosis at 1, 10, and 100 μM SP5031 in HUVECs, MECs, and LECs. After treating with SP5031 for 27 days, we collected mouse organs, including lungs, liver, spleen, and kidney for H&E staining (Figure W6). We did not observe any significant changes within SP5031-treated groups and vehicle (PBS)–treated group. We hypothesize that SP5031 that is primarily blocking cell migration and adhesion, but not proliferation, may have advantage over cell death–inducing conventional chemotherapeutics (Figure W7 and W8).

In this study, SP5031 selectively suppressed VEGFC/VEGFA-induced VEGFR3/VEGFR2 signaling pathways by targeting NRP2 and NRP1 on LECs and BECs. VEGFC-dependent VEGFR3 activation is a major pro-lymphangiogenic signal in LECs [22]. In addition, VEGFR2 is a validated target for VEGFA-dependent angiogenesis and lymphangiogenesis [22]. Thus, SP5031 has the potential to simul-

taneously inhibit lymphangiogenesis and angiogenesis. Recent studies with combination therapies, blocking both lymphangiogenesis and angiogenesis, have shown better outcomes in several experimental models. Targeting cyclooxygenase-2 (COX-2) and prostaglandin E receptors decreased angiogenesis and lymphangiogenesis, improving overall survival rates in breast tumor xenograft models [29]. A combination therapy with short interfering RNA (siRNA) against VEGFC and VEGFA suppressed lymphogenous as well as hematogenous metastasis in mammary tumor models [30]. Bevacizumab combined with a genetic blockade of insulin-like growth factor 1 reduced angiogenesis and lymphangiogenesis in gastric cancer models [31]. Accordingly, multitargeted antilymphangiogenic and antiangiogenic agents have a potential to generate better therapeutics to efficiently inhibit tumor progression and metastasis. To our knowledge, this is the first study targeting tumor-induced lymphangiogenesis and angiogenesis with one short peptide. Previous studies used a combination of two (or more) antibodies, genetic modifications, large proteins, and short interfering RNA [29–31]. The peptide needs to be further modified with sequence mutations for an improved *in vivo* stability, as we discussed previously [32].

SP5031 activity *in vivo* was assessed in a breast tumor xenograft study. SP5031 slowed down tumor growth and blocked lymphangiogenesis and angiogenesis in peritumoral and intratumoral areas of primary tumors in MDA-MB-231 xenograft models (Figure 2). These results suggest that SP5031 could inhibit tumor cell dissemination through stromal LVs and blood vessels in addition to delaying primary tumor growth facilitated by blood vessels (Figure 7, *upper panel*). We further evaluated the *in vivo* activity of SP5031 in tumor-conditioned regional LNs (Figure 3). In this LN model, we observed two to three times larger, more pro-angiogenic, and pro-lymphangiogenic axillary and brachial LNs in TCM-treated animals. SP5031 treatment inhibited the increase in the LN volume and the LVDs and BVDs in the LNs. As shown in Figure 7 (*upper panel*), we can speculate that the inhibition of LN lymphangiogenesis by SP5031 could delay tumor invasion into the LNs by limiting lymphatic flow [21]. At the same time, the inhibition of LN angiogenesis by SP5031 could block the conditioning of metastatic niches in the LNs, thus depriving tumor cells that may have metastasized to the LNs of sufficient oxygen and nutrients [33].

In the proposed mechanism of action of SP5031 (Figure 7, *lower panel*), SP5031 blocks the activities of VEGFR2/3 by binding to NRP1/2. Recently, we have shown that VEGFR2 is expressed on both BECs and LECs, and blockade of VEGFR2 by SP5031 showed dual inhibition of LECs and BECs [34]. With the present data that SP5031 blocks VEGFR3 that is expressed exclusively predominantly on LECs, SP5031 mostly targets VEGFR2 through the binding to NRP1 and partially blocks VEGFR3 through NRP2. NRP1 and NRP2 have three common structural motifs: two CUB homology domains, two coagulation factor V/VIII homology domains, and a MAM domain. In addition to having similar motifs, NRP1 and NRP2 share 44% amino acid sequence identity [35]. Peptide binding to NRP1 and NRP2 blocks complex formation between VEGFR2 and NRP1 (on BECs) and VEGFR3 and NRP2 (on LECs), indirectly inhibiting signaling from VEGFR2 and VEGFR3 in the presence of VEGFA and VEGFC. NRP1/2-mediated inhibition of VEGFR2/3 suggests that SP5031 may synergize with the currently used VEGFA monoclonal antibody (bevacizumab) and the VEGFR2 monoclonal antibody, ramucirumab [36]. At the intracellular level (Figure 7, *lower panel*), SP5031 inhibits FAK and p38MAPK-related proteins. It is known that p38MAPK and HSP27

activate actin reorganization, inducing endothelial cell migration [37]. FAK is central for focal adhesion turnover that is required for endothelial cell adhesion and migration. Thus, the antimigratory and anti-adhesive activities of SP5031 can be explained by its inhibition of FAK and p38MAPK.

Taken together, these findings show that SP5031 is capable of directly tuning lymphangiogenesis and angiogenesis through multi-modal inhibitory mechanisms to improve current antiangiogenic strategies in cancer treatment.

Acknowledgments

References

[1] Carmeliet P and Jain RK (2011). Molecular mechanisms and clinical applications of angiogenesis. *Nature* **473**, 298–307.

[2] Tammela T and Alitalo K (2010). Lymphangiogenesis: molecular mechanisms and future promise. *Cell* **140**, 460–476.

[3] Doeden K, Ma Z, Narasimhan B, Swetter SM, Detmar M, and Dadras SS (2009). Lymphatic invasion in cutaneous melanoma is associated with sentinel lymph node metastasis. *J Cutan Pathol* **36**, 772–780.

[4] Lee AH, Pinder SE, Macmillan RD, Mitchell M, Ellis IO, Elston CW, and Blamey RW (2006). Prognostic value of lymphovascular invasion in women with lymph node negative invasive breast carcinoma. *Eur J Cancer* **42**, 357–362.

[5] Hyung WJ, Lee JH, Choi SH, Min JS, and Noh SH (2002). Prognostic impact of lymphatic and/or blood vessel invasion in patients with node-negative advanced gastric cancer. *Ann Surg Oncol* **9**, 562–567.

[6] Ran S, Volk L, Hall K, and Flister MJ (2010). Lymphangiogenesis and lymphatic metastasis in breast cancer. *Pathophysiology* **17**, 229–251.

[7] Cueni LN, Hegyi I, Shin JW, Albinger-Hegyi A, Gruber S, Kunstfeld R, Moch H, and Detmar M (2010). Tumor lymphangiogenesis and metastasis to lymph nodes induced by cancer cell expression of podoplanin. *Am J Pathol* **177**, 1004–1016.

[8] Tobler NE and Detmar M (2006). Tumor and lymph node lymphangiogenesis—impact on cancer metastasis. *J Leukoc Biol* **80**, 691–696.

[9] Hirakawa S, Brown LF, Kodama S, Paavonen K, Alitalo K, and Detmar M (2007). VEGF-C-induced lymphangiogenesis in sentinel lymph nodes promotes tumor metastasis to distant sites. *Blood* **109**, 1010–1017.

[10] Duong T, Koopman P, and Francois M (2012). Tumor lymphangiogenesis as a potential therapeutic target. *J Oncol* **2012**, 204946.

[11] DeSantis C, Siegel R, Bandi P, and Jemal A (2011). Breast cancer statistics, 2011. *CA Cancer J Clin* **61**, 409–418.

[12] Doyle DM and Miller KD (2008). Development of new targeted therapies for breast cancer. *Breast Cancer* **15**, 49–56.

[13] Kerbel RS (2011). Reappraising antiangiogenic therapy for breast cancer. *Breast* **20**(suppl 3), S56–S60.

[14] Martin M (2011). Understanding the value of antiangiogenic therapy in metastatic breast cancer. *Curr Opin Oncol* **23**(suppl), S1.

[15] Tanne JH (2011). FDA cancels approval for bevacizumab in advanced breast cancer. *BMJ* **343**, d7684.

[16] Paez-Ribes M, Allen E, Hudock J, Takeda T, Okuyama H, Vinals F, Inoue M, Bergers G, Hanahan D, and Casanovas O (2009). Antiangiogenic therapy elicits malignant progression of tumors to increased local invasion and distant metastasis. *Cancer Cell* **15**, 220–231.

[17] Ribatti D (2011). Antiangiogenic therapy accelerates tumor metastasis. *Leuk Res* **35**, 24–26.

[18] Karagiannis ED and Popel AS (2008). A systematic methodology for proteome-wide identification of peptides inhibiting the proliferation and migration of endothelial cells. *Proc Natl Acad Sci USA* **105**, 13775–13780.

[19] Lee E, Rosca EV, Pandey NB, and Popel AS (2011). Small peptides derived from somatotropin domain-containing proteins inhibit blood and lymphatic endothelial cell proliferation, migration, adhesion and tube formation. *Int J Biochem Cell Biol* **43**, 1812–1821.

[20] Tomayko MM and Reynolds CP (1989). Determination of subcutaneous tumor size in athymic (nude) mice. *Cancer Chemother Pharmacol* **24**, 148–154.

[21] Mumprecht V and Detmar M (2009). Lymphangiogenesis and cancer metastasis. *J Cell Mol Med* **13**, 1405–1416.

[22] Hirakawa S, Kodama S, Kunstfeld R, Kajiya K, Brown LF, and Detmar M (2005). VEGF-A induces tumor and sentinel lymph node lymphangiogenesis and promotes lymphatic metastasis. *J Exp Med* **201**, 1089–1099.

[23] Caunt M, Mak J, Liang WC, Stawicki S, Pan Q, Tong RK, Kowalski J, Ho C, Reslan HB, Ross J, et al. (2008). Blocking neuropilin-2 function inhibits tumor cell metastasis. *Cancer Cell* **13**, 331–342.

[24] Kawamura H, Li X, Goishi K, van Meeteren LA, Jakobsson L, Cebe-Suarez S, Shimizu A, Edholm D, Ballmer-Hofer K, Kjellen L, et al. (2008). Neuropilin-1 in regulation of VEGF-induced activation of p38MAPK and endothelial cell organization. *Blood* **112**, 3638–3649.

[25] Tremmel M, Matzke A, Albrecht I, Laib AM, Olaku V, Ballmer-Hofer K, Christofori G, Heroult M, Augustin HG, Ponta H, et al. (2009). A CD44v6 peptide reveals a role of CD44 in VEGFR-2 signaling and angiogenesis. *Blood* **114**, 5236–5244.

[26] Forster-Horvath C, Meszaros L, Raso E, Dome B, Ladanyi A, Morini M, Albini A, and Timar J (2004). Expression of CD44v3 protein in human endothelial cells *in vitro* and in tumoral microvessels *in vivo*. *Microvasc Res* **68**, 110–118.

[27] Kodera Y, Katanasaka Y, Kitamura Y, Tsuda H, Nishio K, Tamura T, and Koizumi F (2011). Sunitinib inhibits lymphatic endothelial cell functions and lymph node metastasis in a breast cancer model through inhibition of vascular endothelial growth factor receptor 3. *Breast Cancer Res* **13**, R66.

[28] Karaman MW, Herrgard S, Treiber DK, Gallant P, Atteridge CE, Campbell BT, Chan KW, Ciceri P, Davis MI, Edeen PT, et al. (2008). A quantitative analysis of kinase inhibitor selectivity. *Nat Biotechnol* **26**, 127–132.

[29] Xin X, Majumder M, Girish GV, Mohindra V, Maruyama T, and Lala PK (2012). Targeting COX-2 and EP4 to control tumor growth, angiogenesis, lymphangiogenesis and metastasis to the lungs and lymph nodes in a breast cancer model. *Lab Invest* **92**, 1115–1128.

[30] Shibata MA, Morimoto J, Shibata E, and Otsuki Y (2008). Combination therapy with short interfering RNA vectors against VEGF-C and VEGF-A suppresses lymph node and lung metastasis in a mouse immunocompetent mammary cancer model. *Cancer Gene Ther* **15**, 776–786.

[31] Li H, Adachi Y, Yamamoto H, Min Y, Ohashi H, Ii M, Arimura Y, Endo T, Lee CT, Carbone DP, et al. (2011). Insulin-like growth factor-I receptor blockade reduces tumor angiogenesis and enhances the effects of bevacizumab for a human gastric cancer cell line, MKN45. *Cancer* **117**, 3135–3147.

[32] Rosca EV, Koskimaki JE, Rivera CG, Pandey NB, Tamiz AP, and Popel AS (2011). Anti-angiogenic peptides for cancer therapeutics. *Curr Pharm Biotechnol* **12**, 1101–1116.

[33] Carlini MJ, De Lorenzo MS, and Puricelli L (2011). Cross-talk between tumor cells and the microenvironment at the metastatic niche. *Curr Pharm Biotechnol* **12**, 1900–1908.

[34] Koskimaki JE, Lee E, Chen W, Rivera CG, Rosca EV, Pandey NB, and Popel AS (2012). Synergy between a collagen IV mimetic peptide and a somatotropin-domain derived peptide as angiogenesis and lymphangiogenesis inhibitors. *Angiogenesis* **16**, 159–170.

[35] Bagri A, Tessier-Lavigne M, and Watts RJ (2009). Neuropilins in tumor biology. *Clin Cancer Res* **15**, 1860–1864.

[36] Spratlin J (2011). Ramucirumab (IMC-1121B): monoclonal antibody inhibition of vascular endothelial growth factor receptor-2. *Curr Oncol Rep* **13**, 97–102.

[37] Nguyen A, Chen P, and Cai H (2004). Role of CaMKII in hydrogen peroxide activation of ERK1/2, p38 MAPK, HSP27 and actin reorganization in endothelial cells. *FEBS Lett* **572**, 307–313.

[38] Harrell JC, Dye WW, Allred DC, Jedlicka P, Spoelstra NS, Sartorius CA, and Horwitz KB (2006). Estrogen receptor positive breast cancer metastasis: altered hormonal sensitivity and tumor aggressiveness in lymphatic vessels and lymph nodes. *Cancer Res* **66**, 9308–9315.
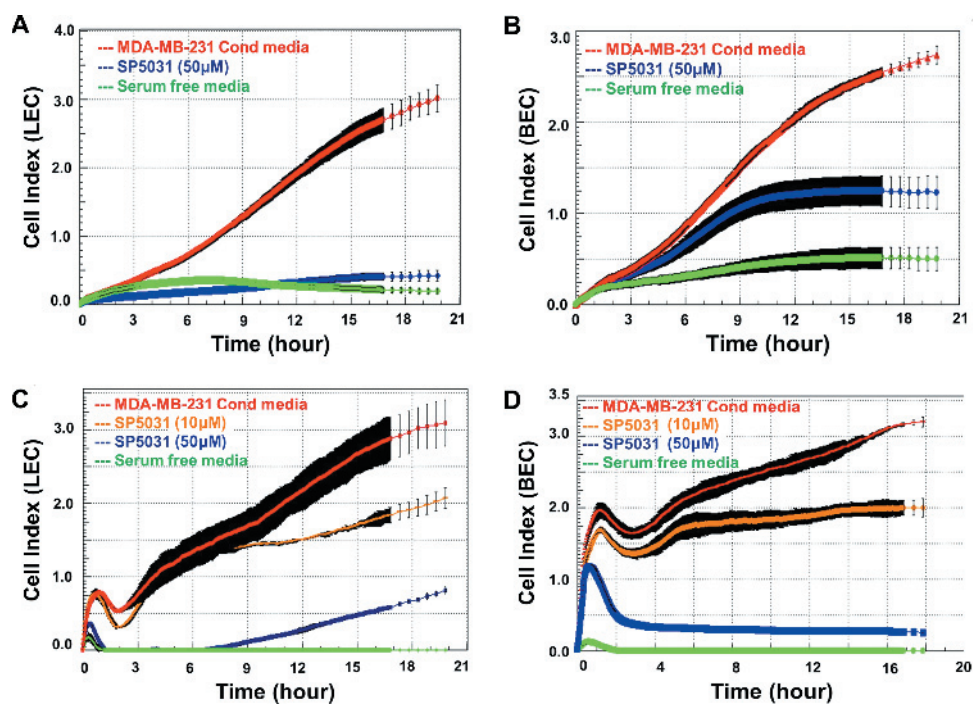
Figure W1. Real-time analysis of LEC/BEC migration and adhesion. SP5031 was tested in TCM-induced LEC/BEC migration and adhesion, using RTCA System combined with CIM-plate and E-plate. Cell indices are proportional to the number of migrated or adhesive LECs/BECs (A) Real-time LEC migration in TCM with our without SP5031 (CIM-plate). (B) BEC migration. (C) Real-time LEC adhesion (E-plate). (D) BEC adhesion.
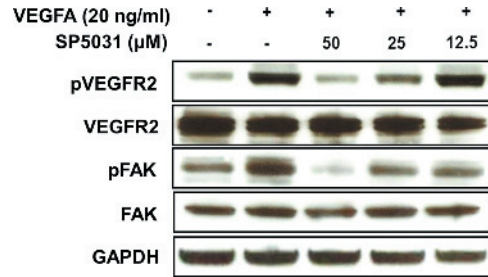
Figure W2. VEGFA signaling with SP5031 treatment in MEC. HUVECs are routinely used in endothelial cell Western blot assays (in Figure 5*A*) but, because of their venous origin, may not adequately reflect micro-capillaries of tumors. As an additional study, we look at the effect of SP5031 in MECs. VEGFA-induced phosphorylation of VEGFR2 (Y1175) and FAK (4G10) was blocked by SP5031 in MECs. GAPDH was measured as a loading control.
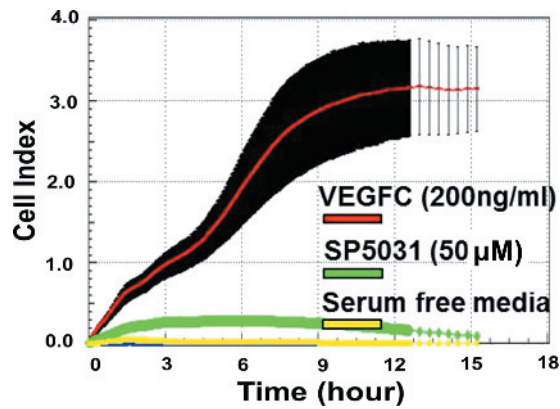

Figure W3. VEGFC-induced LEC migration. LEC migration was measured in real-time with or without SP5031 treatment. SP5031 inhibited VEGFC-dependent LEC migration.
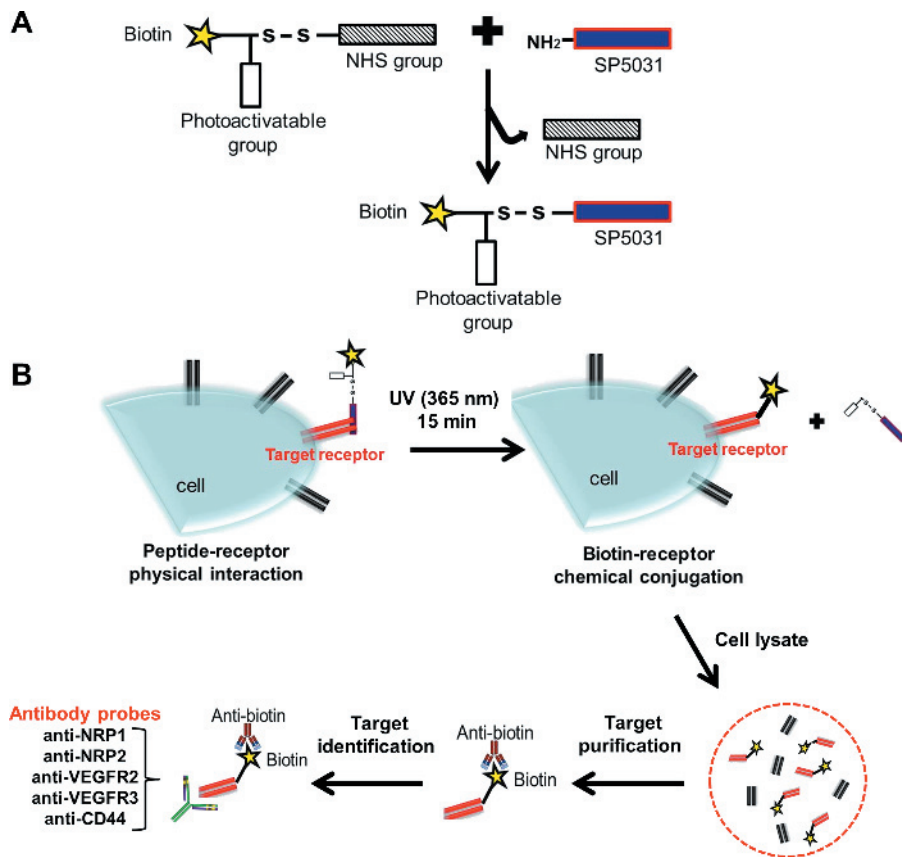
Figure W4. Sulfo-SBED cross-linking methodology. (A) A Sulfo-SBED Biotin Label Transfer Reagent (Thermo Scientific Inc) has three functional groups, including an amine-reactive NHS-ester group, a UV-activatable aryl azide group, and a biotin group. The peptide was reacted with Sulfo-SBED in PBS at room temperature for 2 hours, in the dark. (B) Probe-conjugated peptide was added to HUVECs or LECs in PBS in a 24-well plate and the plate was exposed in UV (365 nm) for 15 minutes. Then, the biotin groups are reacted with target receptors, making chemical bonds: The biotinylated target receptors were purified by using anti-biotin and then probed by target receptor antibodies.
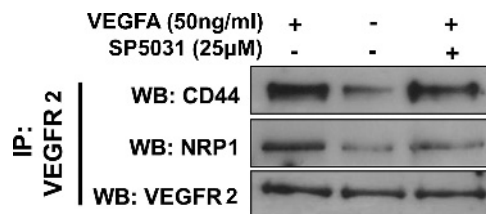

Figure W5. VEGFR2/CD44 or VEGR2/NRP1 complex formation with SP5031 treatment. VEGFA induces VEGFR2 and CD44 complex formation as well as VEGFR2 and NRP1 complex in HUVECs. SP5031 binds to NRP1 and dissociates the VEGFR2 and NRP1 complex formation. However, SP5031 does not inhibit VEGFR2 and CD44 complex formation, as SP5031 has no interaction with CD44.
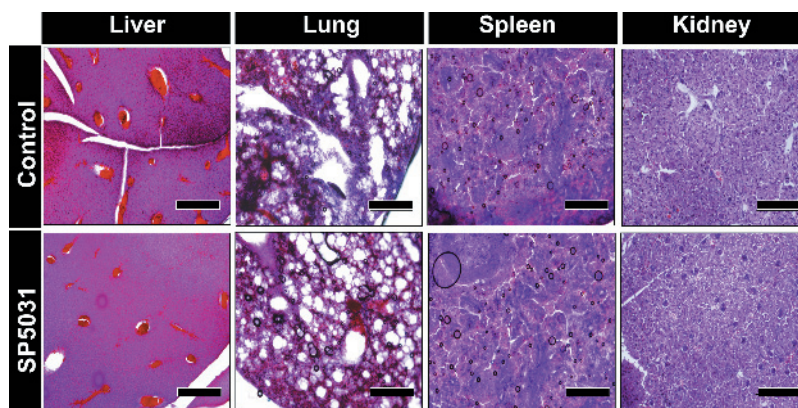
Figure W6. SP5031 is not toxic to normal tissues as seen by histopathology. Histopathological examination of liver, lung, spleen, and kidney was performed by H&E staining. No significant morphologic changes were seen in these organs from animals treated with SP5031, compared to the organs from the control group of animals. Scale bars represent 500 μm.
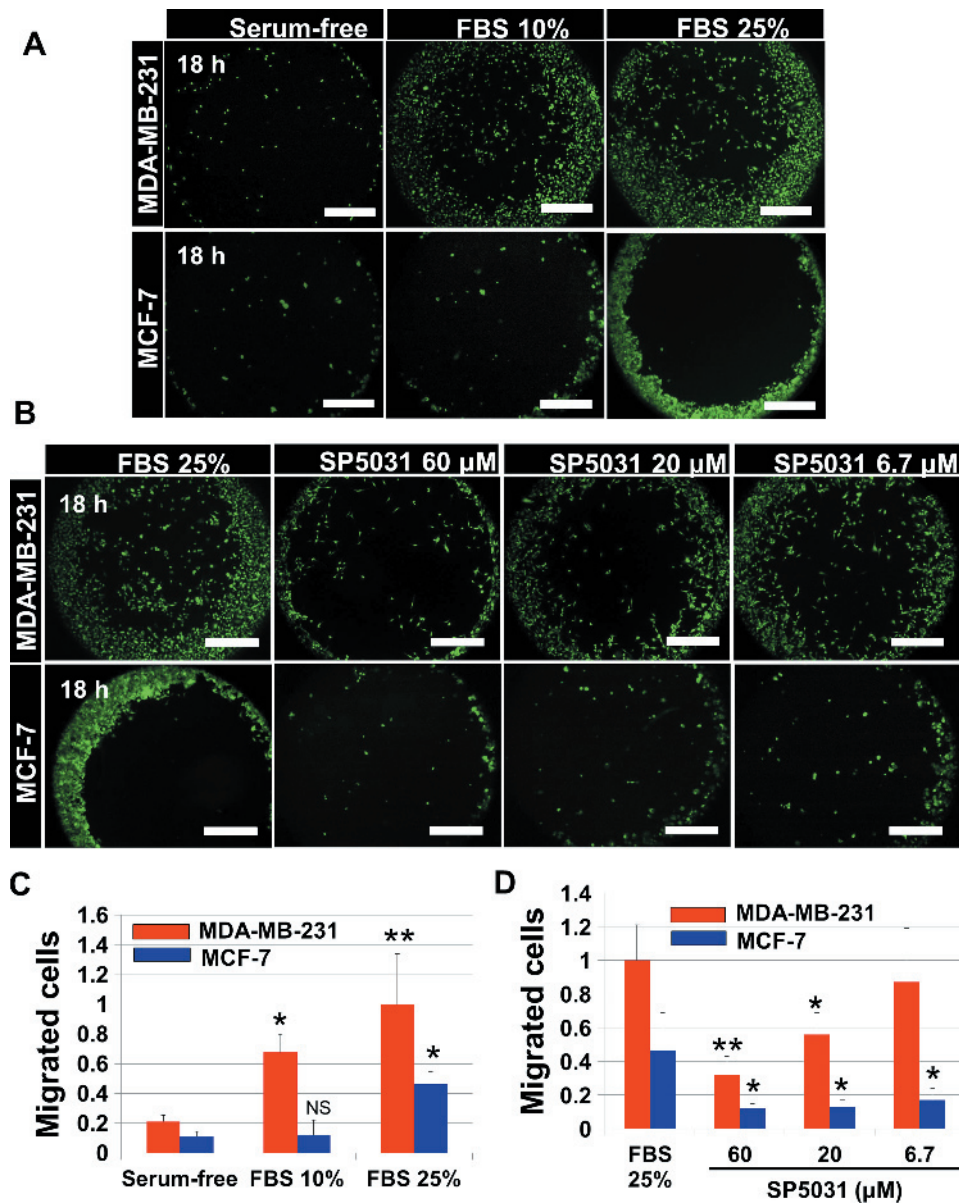
Figure W7. SP5031 inhibits migration of both MDA-MB-231 and MCF-7 cells. The effect of SP5031 on cancer cell migration on fibronectin-coated Platypus migration plates was tested. (A) Optimization of the experimental condition. MCF-7 is relatively passive in migration, compared to MDA-MB-231 cells; thus, we could not see a significant MCF-7 migratory induction in 10% FBS. Twenty-five percent FBS was determined to adequately induce migration of both cell lines. Scale bars represent 500 μm. (B) SP5031 inhibited migration (at 18 hours) of MDA-MB-231 and MCF-7 cells. Scale bars represent 500 μm. (C) Quantification of A by measuring fluorescence. *$P < .05$ and **$P < .01$ *versus* serum-free condition. NS represents "not significant." (D) Quantification of B. SP5031 potently inhibited migration of both cells from both types of breast cancer. *$P < .05$ and **$P < .01$ *versus* 25% FBS induction. Fluorescent intensity of the migrated MDA-MB-231 cells (25% FBS) was set at 1.0.
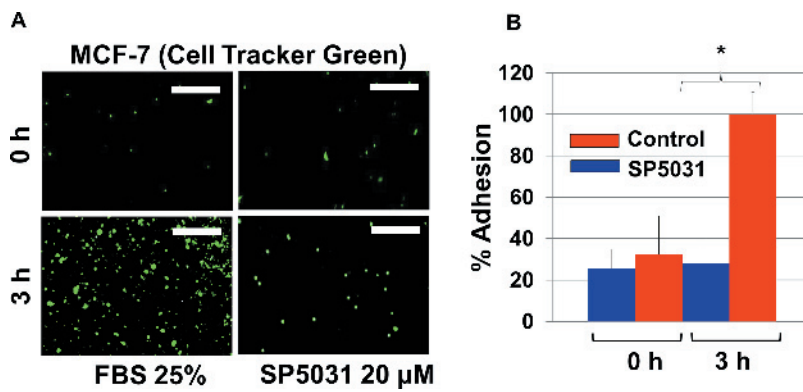
Figure W8. SP5031 inhibits adhesion of MCF-7 cells. The effect of SP5031 on MCF-7 cell adhesion on fibronectin-coated well plates was tested. (A) CellTracker Green–labeled MCF-7 cells adhered within 3 hours in 25% FBS. SP5031 treatment potently blocked the adhesion. (B) Quantification of A. *P < .05 *versus* 25% FBS induction without the peptide.